AIAA JOURNAL
Vol. 48, No. 8, August 2010

Numerical Simulations of Shock Focusing over Concave Surfaces

David Taieb,* Guillaume Ribert,† and Abdellah Hadjadj‡
Complexe de Recherche Interprofessionnel en Aérothermochimie, 76801 Saint Etienne du Rouvray, France

DOI: 10.2514/1.J050199

This paper describes the numerical study of a shock focusing, that is, a planar shock wave impacting a concave surface. Cylindrical and parabolic reflectors are studied for different curvatures, depths and incident Mach numbers. Computations are carried out using a high-order low-dissipation bandwidth-optimized weighted essentially nonoscillatory method and both inviscid and viscous two-dimensional flow models are considered. The obtained results agree well with the experimental observations made by Skews et al. (Skews, B. W., Kleine, H., Barber, T., and Iannuccelli, M., "New Flow Features in a Cavity During Shock Wave Impact," *16th Australian Fluid Mechanics Conference*, Univ. of Queensland, Brisbane, Australia, 2007) and Izumi et al. (Izumi, K., Aso, S., and Nishida, M., "Experimental and Computational Studies Focusing Processes of Shock Waves Reflected from Parabolic Reflectors," *Shock Waves*, Vol. 3, No. 3, 1994, pp. 213–222) for the parabolic one. In the case of cylindrical reflectors, shocks interaction and fine structures as Kelvin–Helmholtz instabilities are recovered, and the computed angles of the transition from an inverse Mach reflection to a transitional regular reflection compare favorably with the analytical model of Ben–Dor (Ben–Dor, G., *Shock Wave Reflection Phenomena*, Springer–Verlag, New York, 1992) for relatively weak incident shock waves ($M_s \leq 2$). In the case of parabolic reflectors, the three types of focalization process are addressed and their own structure analyzed.

Nomenclature

a	=	speed of sound
E_i	=	internal energy
E_k	=	kinetic energy
E_t	=	total energy
h	=	enthalpy
h_t	=	total enthalpy
M_s	=	incident shock Mach number
V_p	=	piston velocity
c	=	curvature of the parabolic cavity
L	=	depth of the parabolic cavity
X	=	absciss inside the domain
Y	=	ordinate inside the domain
α_c	=	critical angle
V_1	=	shock induced flow velocity
C	=	compression wave
F	=	focusing wave
H	=	Mach stem
I	=	incident shock
J	=	jet
M	=	main reflected shock
R	=	reflected shock
S	=	slipstream
T	=	triple point
V	=	wall vortex
W	=	shock at wall
γ	=	heat capacity ratio
θ	=	transition angle

Subscripts

0	=	state at rest
1	=	state postshock

I. Introduction

THE reflection of a planar shock over a concave surface has attracted the interest of many researchers during the past few years because this type of reflection yields a truly complex and unsteady flow. Consequently, the understanding of this unsteady phenomenon will contribute to the knowledge of more complex process like explosion and blast waves. Basically, the reflection of a shock wave occurs when a planar shock encounters a cylindrical or parabolic concave wall (Fig. 1) and reflects from it forming a locally high-pressure region near the focusing locus. This process may be used to produce very strong shock waves and initiate detonations. The general phenomena of shock focusing in gaseous media were reviewed by Grönig [1] and a comprehensive study of shock focusing was carried out experimentally and numerically by Izumi et al. [2] for a range of parabolic reflectors of different curvatures. Several focusing types were identified with a classification of the shock focusing process according to the incident shock Mach number and reflectors shape. Regarding the dynamics of the shock wave reflection, researchers have focused their studies on the type of transition, from Mach to regular reflection. Depending on the incident Mach number and the cavity shape, direct or inverse Mach reflections can be obtained. Later, when the wedge becomes steep enough, the Mach reflection changes into a transitional regular reflection. The majority of this work, mostly done by Ben-Dor and coworkers, is summarized in his monograph [3]. In a recent article of Skews and Kleine [4], additional information of shock focusing on cylindrical cavities have been provided experimentally. In particular, the very interesting flow patterns generated in the postfocus state are highlighted, showing clearly a jet development and a shear-layer exhibiting a two-dimensional Kelvin–Helmholtz (KH) instability at the early stages of the focusing process[§]. This jet development has been also noticed by Shugaev and Shtemenko [5], Sturtevant and Kulkarny [6] and some figures provided in the articles of Izumi et al. [2] or Liang et al. [7] let also imagine these flow features. Similar trends are observed by Gelfand et al. [8] who studied experimentally the detonation/deflagration processes initiated by semicylinder and

Received 9 September 2009; revision received 2 February 2010; accepted for publication 16 March 2010.

*Ph.D. Student, CNRS UMR 6614, INSA de Rouen, Campus du Madrillet BP12; taieb@coria.fr.

†Associate Professor, CNRS UMR 6614, INSA de Rouen, Campus du Madrillet BP12; ribert@coria.fr. Senior Member AIAA.

‡Professor, CNRS UMR 6614, INSA de Rouen, Campus du Madrillet BP12; hadjadj@coria.fr.

§Private communication with B. W. Skews, January 2010.

parabolic focusing elements. The two-dimensional roll-up and pairing mechanisms observed for the KH instabilities have been found for weakly compressible shear layers [9,10]. Besides linear stability analysis [11–13] of temporal and spatial stability problems highlighted the two-dimensional nature of the most amplified disturbances up to convective Mach numbers of 0.6. For higher Mach number KH instabilities are inhibited and the flow becomes strongly three-dimensional [14,15]. From numerical point of view, the physical modeling of such complex flows requires an accurate description of both shocks and shear layers. In this context, Liang et al. [7] used a finite volume approach with a second-order total variation diminishing (TVD) scheme of Yee and Harten [16]. They simulated a shock wave ($M_s = 1.2$ or 1.85) impacting a parabolic reflector and compared their results with experimental schlieren pictures. The reflected shock wave observed in these experiments has been well reproduced, however, the associated slipstream instabilities were missed. A similar failure was noted by Skews et al. [17] when they tried to reproduce their experiments using Fluent software with a third-order MUSCL scheme. All these simulations have been realized for two-dimensional configurations as they are focused on the early stages of the focusing process.

In spite of many experimental and numerical studies on the subject, the shock focusing mechanism and its related pressure-peak generation are quite complex. The fundamental knowledge of supersonic flow physics in the presence of shock reflection at concave walls, shock/shock and shock/shear layer interactions is still needed. The objective of the present article is to simulate the shock focusing phenomenon using a high-order low-dissipation shock capturing scheme (weighted essentially nonoscillatory, or WENO, type) in order to bring more light and understanding to the complex phenomenon of shock focusing and transition over concave surfaces. The paper is organized as follow: a brief description of the numerical solver together with the geometrical configurations is given in Sec. II. Cylindrical reflectors are studied in Sec. III for different values of the incident Mach number using both inviscid and viscous computations. Further analysis are performed in Sec. IV for parabolic reflectors with various curvature and depth of the cavity, leading to the conclusion given in Sec. V.

II. Numerical Solver and Flow Configurations

The numerical simulation of the shock focusing was performed by applying the WENO method [18,19] available within an inhouse two-dimensional structured code written in generalized Cartesian coordinates. Even though the WENO method has the great advantage of representing shock waves and other discontinuities very sharply, there are several disadvantages especially for viscous simulations. As soon as the shock wave propagates and interacts with viscous layers, the mixing front is spread over several mesh points, and strong dumping due to the numerical dissipation are found near contact discontinuities. Compared with the fourth-order Padé scheme, a spectral analysis of the fifth-order WENO scheme exhibits a limited behavior for properly resolving the very fine flow structures. In the present paper, the bandwidth-optimized WENO method proposed by Martín et al. [20], is applied to the shock focusing in air. This method has been already successfully applied to the computation of shock-turbulence and shock-mixing interactions [20]. It is a symmetry optimized extension of the fifth-order Shu's WENO method [18,19] referred to us as WENO5-SOL (symmetry-optimized-limiter), which yields a rather steep representation of shocks and discontinuities. The detailed description of the SOL procedure may be found in the original work of Martín et al. [20] and Taylor et al. [21]. Viscous fluxes are computed using a compact fourth-order central scheme [22], whereas time is advanced using an explicit third-order Runge–Kutta TVD approach [19].

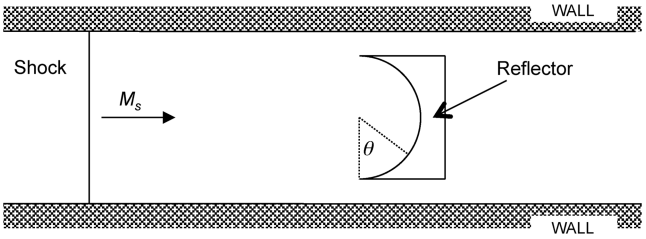

Fig. 1 Schematic illustration of the shock focusing configuration.

A schematic representation of the experimental setup is shown in Fig. 1, where an initial planar shock wave generated by a shock tube impacts the test piece and gives rise to very complex flow structures inside the cavity. Obviously, the strength of the shock as well as the shape of the reflector play an important role in the evolution of different flow features. Numerical computations are presented for two cases, a cylindrical reflector with 64 mm radius and a series of parabolic reflectors having different depths and curvatures. The focusing processes are qualitatively compared with the experiments of Skews and Kleine [4] in the case of cylindrical reflectors, and to the experimental work of Izumi et al. [2] for parabolic reflectors. Accordingly, different mesh strategies are adopted depending on the shape of the considered geometry (Fig. 2).

1) For cylindrical reflectors, the mesh contains 1.7 million points. The concavity of the physical domain yields an array of degenerated cells along the bisector to fit the reflector within a topologically equivalent squared computational domain. These cells having a triangular shape (see Fig. 2) are generated with two colinear edges of a squared mesh. Preliminary numerical tests showed that the possible resulting perturbations caused by the nonalignment of the shock with the mesh [23] through this array of cells are negligible. Compared with the experiment apparatus, the gap between the test cavity and the horizontal boundaries of the shock tube (walls in Fig. 1) is removed. Consequently, the inlet lip of the cavity is tangent to the computational domain and the thickness of the lip profile is no longer considered in the simulation. Subsequently, the initial compression waves described by Skews and Kleine [4] are missed in the computation. However, one can argue that the signal emanating from the cavity corner is of limited influence specifically at later stage of flow evolution as it does not much affect the dynamics of the shock reflection and the focusing process as well [4].

2) For the parabolic reflectors, studied experimentally by Izumi et al. [2], the mesh contains 0.85 million points. Unlike cylindrical reflectors, parabolic reflectors are topologically equivalent to a squared box having a small distortion of the cells along the domain. However, the shape of the reflector involves a finite angle at the cavity inlet and small reflected shocks may appear and interact with the upper boundary. The computational domain is then extended further

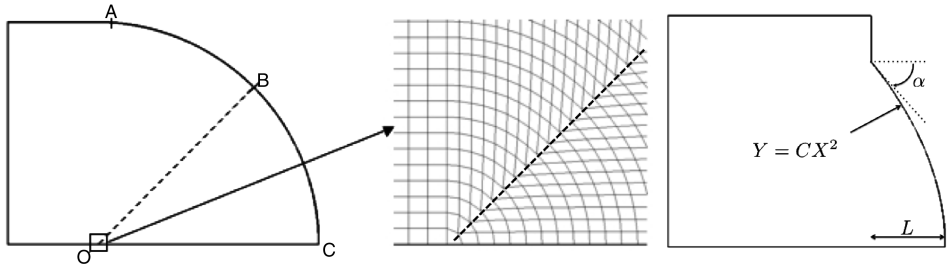

a) Cylindrical domain and mesh **b) Parabolic**

Fig. 2 Computational domain and mesh strategy for the shock focusing problem.

Table 1 Transition angle for different mesh sizes (in million of cells)

Mesh size	$\theta_{\text{comp}} \pm 1°$
1.0	62.66
1.7	60.37
2.4	60.96
Theory	59.24

downstream to avoid shock reflection at the inlet. Note that due to the wall angle, a Mach reflection appears soon contrary to the observation made by Skews et al. [17] in the case of a cylindrical reflector.

Owing to the symmetry of the two configurations, only half of the physical domain is computed, with a symmetry boundary condition imposed at the horizontal centerline. No special treatment is applied near the solid walls. A mesh refinement study has been realized for three different mesh sizes: 1.0, 1.7 and 2.4 million cells. All other things being equal, flow structures have been found quasi unchanged. To assess this behavior, the angle of the invMR → TRR transition is computed and compared with the theoretical model proposed by Ben–Dor [3] and developed in the next section. In Table 1, a very good agreement is found from the 1.7 million mesh points. A slip boundary condition is imposed at the cavity wall, except in the case of viscous simulations where the nonslip conditions are fixed along the wall. Supersonic boundary conditions are prescribed at the inlet using Rankine–Hugoniot relations of a moving shock into an ambient air at a given Mach number. The initial conditions are generated using a piston code in a closed box on a mesh equivalent to that of the shock focusing simulation. In this case, the Mach number of the incident shock M_s is related to the piston velocity V_p through the relation [24]

$$(M_s^2 - 1)/M_s = \frac{1}{2}(\gamma + 1)(V_p/a_0) \tag{1}$$

where a_0 is the speed of sound in the driven gas (fluid at rest).

III. Cylindrical Reflectors

Skews and Kleine's [4] experiments have been considered for the study of cylindrical reflectors. Experimental tests are conducted in a shock tube having a section of 150 mm high and 75 mm wide and a test piece of 64 mm radius and only flow visualizations are currently available. The test-case with an incident shock Mach number of 1.38 is considered hereafter because the flow exhibits nonlinear effects due to the shock propagation, wall interaction and purely viscous postfocus phenomena. As suggested by Skews and Kleine, the description of the flow may be divided into two phases, corresponding to different aspects of the interaction. The first is the reflection of the shock wave at walls and the second corresponds to the focusing process. From a numerical point of view, the early stages of the shock propagation can be described by inviscid computations using standard shock-capturing schemes (second-order TVD, third- or fifth-order WENO schemes) because the interaction between the incident shock and the emerging boundary-layer is assumed to be very weak. However, at later stages, viscous effects are no longer negligible, in particular when the reflected shock initiates shear layers which quickly evolve in KH instabilities. Accurate solutions of the full Navier–Stokes system are therefore needed.

From an energetic point of view, a moving shock into ambient air separates two energetic states: E_t^0 (gas at rest) and E_t^1 (postshock) with $E_t^1 > E_t^0$. E_t is the total energy, which is the sum of internal (E_i) and kinetic (E_k) energy. Because of the total energy balance, once the incident shock (I) enters the cavity, E_i and E_k increase close to the wall leading to weak compression waves and a curved shock, respectively. Further downstream inside the cavity, the curvature of I increases due to the shape of the wall (Fig. 3a), i.e., the foot of I is moving faster than its center until a sudden transition from regular to inverse Mach reflection (invMR) occurs. Basically, this shock system consists of a Mach stem (H) which correspond to the foot of the incident shock, a reflected shock (R) which is created from a sequence of compression waves, and a slipstream (S), which extends away from the cavity wall (Fig. 3b). R and S are then a consequence of the reflection of the initial shock at the transition, i.e., a release of

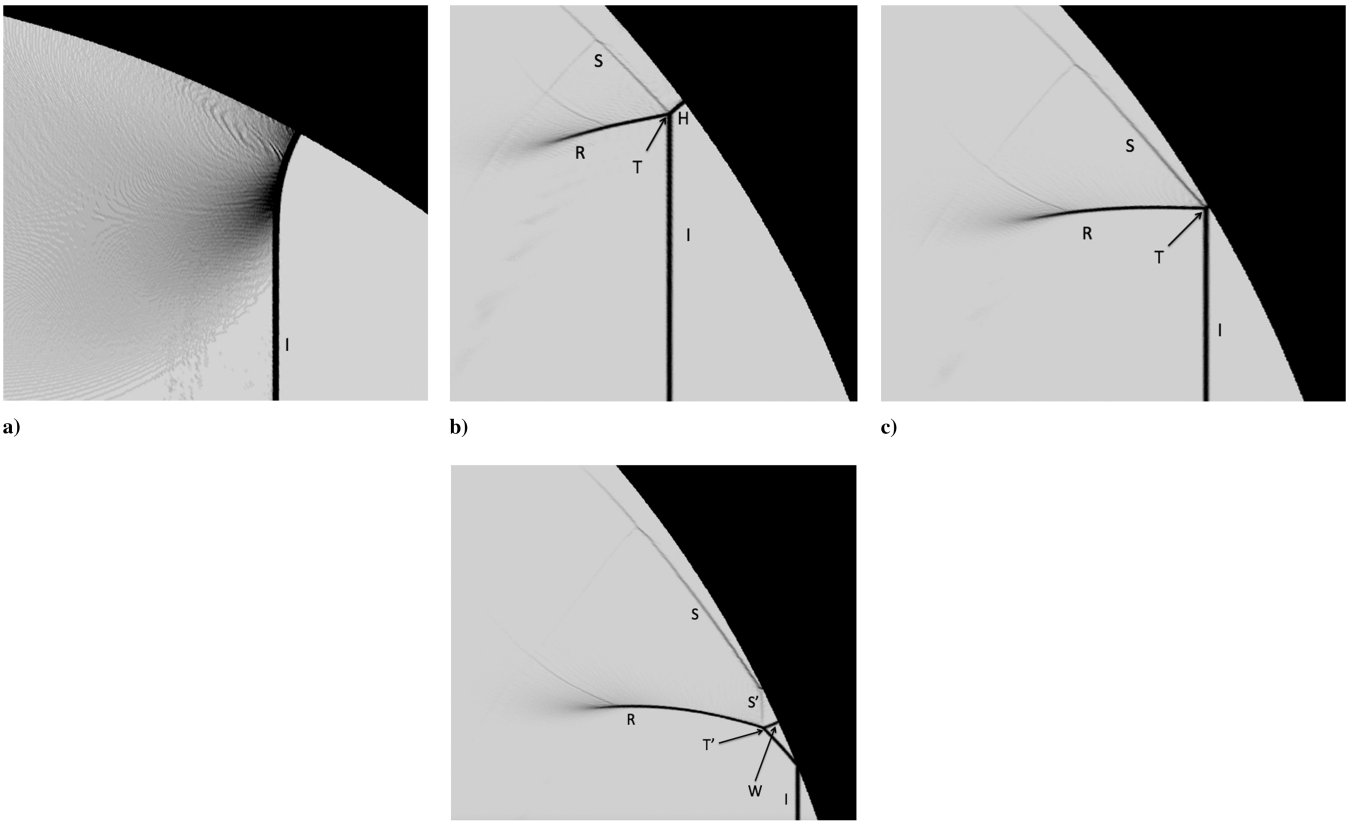

a) b) c) d)

Fig. 3 Incident shock wave curvature and invMR → TRR transition.

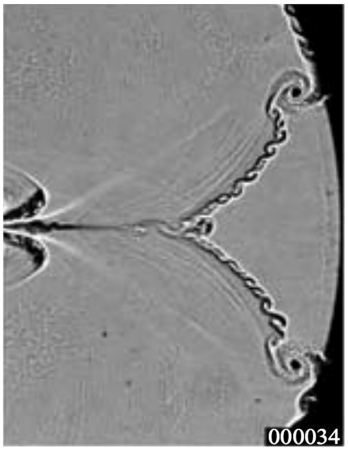

Fig. 4 Focusing process: image courtesy of Skews and Kleine [4].

energy. Another consequence is that I is now going faster than H. This set of waves are connected through a triple point (T) which moves deeper inside the cavity until it collides the reflecting surface (Fig. 3c). At this stage, the Mach stem has disappeared and T exhibits a peak of pressure which corresponds to the maximum of E_i and E_k; note that the maximum of $\nabla h_t = \nabla(h + E_k)$, with h the enthalpy of the system, is located in R. The transitional regular reflection (TRR) is then formed until the incident shock hits the bottom of the cavity (Fig. 3d). The nature of the TRR is driven by the pressure peak which detaches S and modify the pressure distribution. A new triple point (T') is then created and links together the initial reflected wave R, the new reflected wave (R'), the wall shock (W) and the secondary slipstream (S'). This sequence of events has been simulated using three variants of WENO schemes, namely the third-order WENO3, the fifth-order WENO5 and the fifth-order WENO5-SOL schemes with an Euler approach. It is worth noticing that all schemes reproduce the invMR $\rightarrow$ TRR transition as shown in the experiments, with more or less accuracy of the shock thickness.

A. Description of the Shock Focusing Process

According to Skews and Kleine [4], once the focusing process happen, i.e., the incident shock impacts on the cavity giving birth to a focusing wave F, a resulting jet appears inside the cavity by interaction of the secondary slipstream S'. The jet evolves in a mushroom shape with very fine structures at its top. The slipstreams also interact with the near-wall structures leading to a quasi-steady complex vortex. Finally, these shear layers develop KH instabilities (see Fig. 4).

Here again, these flow features have been simulated with the three variants of WENO schemes using inviscid approach and the main trend is recovered. Once the wall reflects the incident shock I, the two

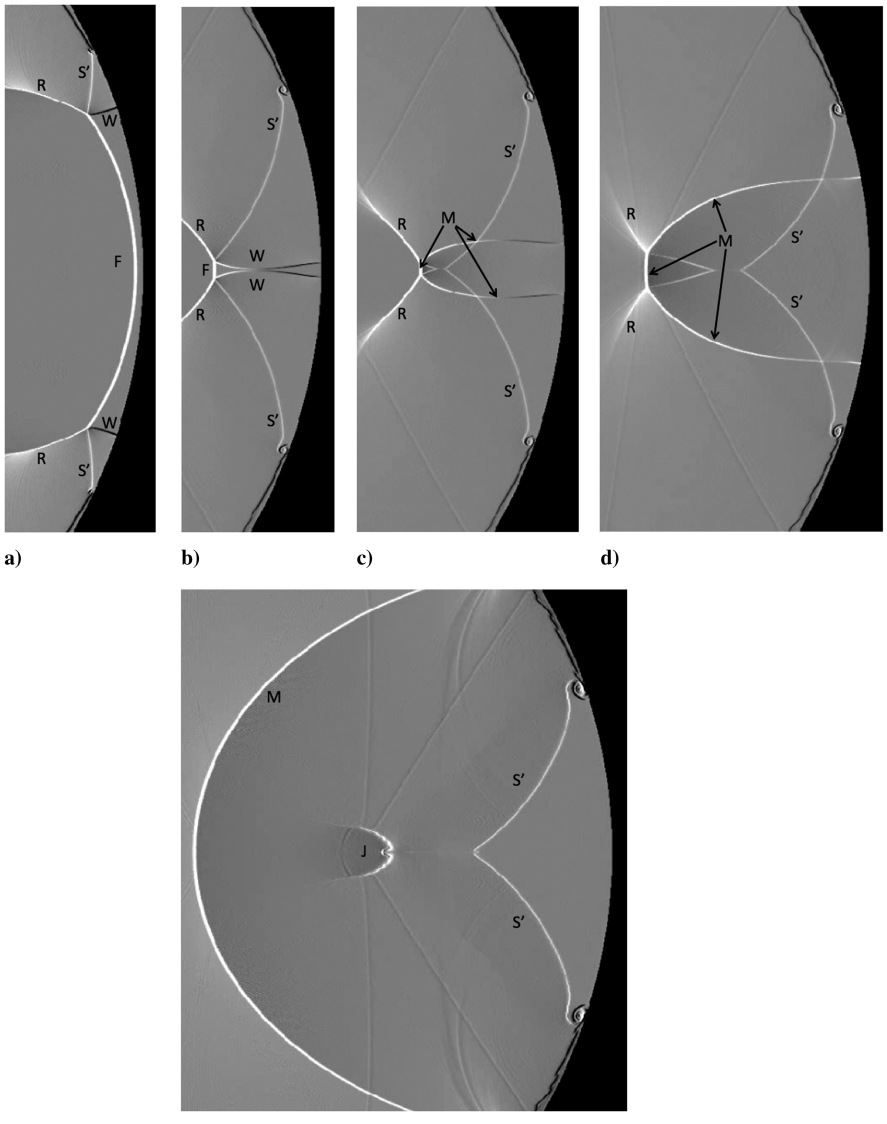

a) b) c) d)

e)

Fig. 5 Sequences of the shock focusing process.

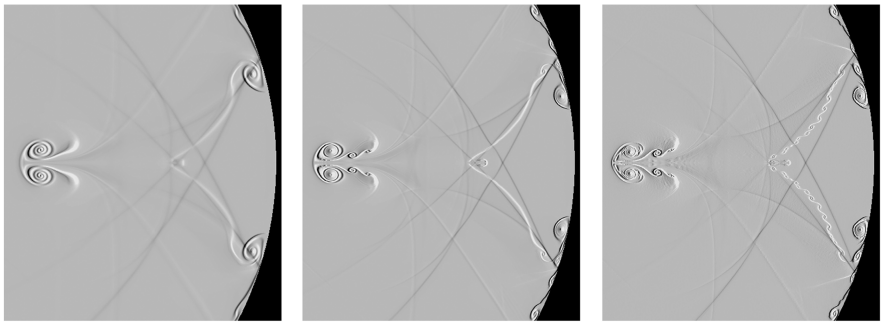

a) WENO3 b) WENO5 c) WENO5-SOL

Fig. 6 Numerical schlieren pictures of the focusing process using three numerical schemes.

reflected waves R' merge and form a focusing wave F moving upstream toward the cavity entrance (Fig. 5a). In the meantime the near-wall shocks (W) move toward the symmetry line and a small vortex appears on the base of the sliplines S'. The height of the shock wave F decreases as W evolves, the sliplines being attached to the triple point (Fig. 5b). When the focusing process occurs, the two near-wall shocks collapse into a single reflected shock (M), the sliplines intercept each other (Fig. 5c) and split into two parts. The first separates a low-speed region, which is created when M moves toward the entrance, from a higher speed region (Fig. 5d). Because of this flow configuration, KH instabilities may appear on S'. The second part of S', corresponding to the mushroom legs, remains attached to the triple point (Fig. 5e). In Fig. 5d, as M moves upstream, the hight of the focusing wave increases and bends as well. In Fig. 5e, when the first reflected wave R disappeared, a strong jet (J) develops. As expected, comparison of different numerical schemes (see Figs. 6) reveals the dissipative behavior of WENO3 because the KH instabilities are not well resolved. Nevertheless, the near-wall vortex (V) is relatively well located. Results of WENO5 show an improvement in the description of the mushroom but KH instabilities are not yet recovered. Indeed, with WENO5 the near-wall structures are better described but the main vortex V detaches from the sliplines. It is clear that an accurate resolution of these structures requires a precise numerical scheme already observed by Shi et al. [25] for the fifth- and ninth-order WENO numerical schemes. Instabilities are then undoubtedly related to the viscosity introduced by the numerical scheme as already point out by Samtaney and Pullin [26] or Shi et al. [25]. Comparison of an experiment picture and Navier-Stokes results are given in Fig. 7. With Navier–Stokes computations, the interaction of the sliplines is better described, the vortex V is well located and the KH instability is developed when the WENO5-SOL is used. Obviously, at this stage of the focusing process viscous effects are the major ingredients in the description of those phenomena.

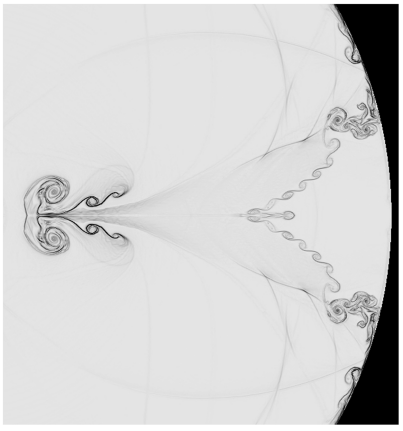

Fig. 7 Focusing process, present work: Navier–Stokes computation with WENO5-SOL.

B. Effect of the Incident Mach Number on the Focusing Process

Increasing the incident Mach number leads to similar results for both Euler and Navier–Stokes computations. Numerical schlieren pictures presented in Fig. 8 show the focusing process when the mushroom edge detaches from the focusing wave F. Three incident Mach numbers are studied: $M_s = 1.38$, 2, and 5. With the inviscid formulation, the near-wall vortices V are not attached to the sliplines and move deeper into the cavity. For a higher Mach number, near-wall vortices progress faster toward the bottom of the concave region. For the case of $M_s = 2$ (Fig. 8b), these vortices are very close to the symmetry plane and perturb S' as time evolves. For the case of $M_s = 5$ (Fig. 8d), the sliplines are totally destroyed as the vortices from each side of the flow interact. Simulations including viscous effects have been also realized and the corresponding case of $M_s = 2$ is shown in Fig. 8c. Compared with the inviscid case, the main difference is the location of V which stays attached to S'. Near-wall structures are also very different as the reflected shock M interacts with the boundary layer creating small vortices when it moves upstream toward the entrance. The case $M_s = 5$ with viscous terms is not shown here as it exhibits similar behaviors to those of the Euler case. Indeed, increasing M_s leads to increase the Reynolds number, i.e., to reduce the viscous effects. The flow structure is then much more complex. Note that increasing the Mach number leads also to common behaviors: KH instabilities develop on the mushroom legs and the focusing wave is not as curved as in the case $M_s = 1.38$.

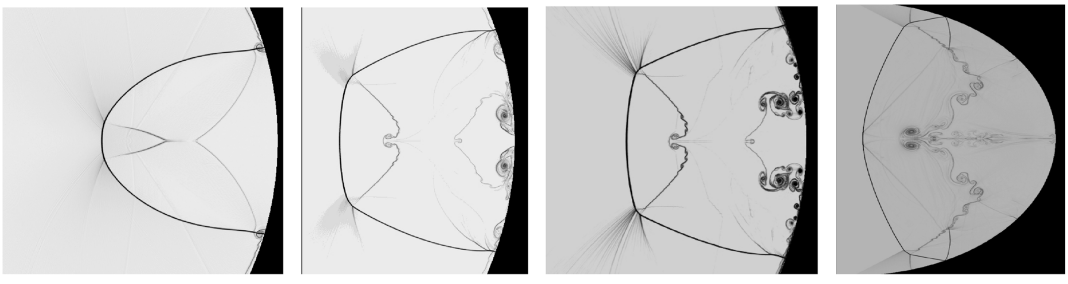

a) M_s = 1.38 b) M_s = 2 c) M_s = 2, viscous d) M_s = 5

Fig. 8 Numerical schlieren pictures of the focusing jet when the mushroom legs detach from the focusing shock.

Table 2 Comparaison of the transition angle

M_s	$\sin(\theta)/\theta$	θ_{theo}	$\theta_{\text{comp}} \pm 1°$
1.38	0.831	59.24	60.37
1.8	0.791	66.29	66.68
2	0.784	67.49	69.57
3	0.777	68.64	73.58

Besides, a small jet always faces the bottom of the cavity indicating a stagnation point.

C. Prediction of the invMR → TRR Transition

According to Ben-Dor's model [3], an analytical prediction of the invMR → TRR transition angle (θ) over cylindrical concave surfaces can be obtained using the following relation:

$$\frac{\sin(\theta)}{\theta} = \frac{M_s}{V_{10} + A_{10}} \tag{2}$$

$A_{10} = a_1/a_0$ where a_0 and a_1 represent the local speeds of sound ahead and behind the incident shock wave, respectively. $V_{10} = V_1/a_0$ with V_1 the shock induced flow velocity, and M_s is the incident shock wave Mach number. For a perfect gas, V_{10} and A_{10} are expressed as:

$$V_{10} = \frac{2(M_s^2 - 1)}{(\gamma + 1)M_s} \tag{3}$$

$$A_{10} = \frac{\gamma - 1}{\gamma + 1}\frac{1}{M_s}\left(\frac{2\gamma}{\gamma - 1}M_s^2 - 1\right)^{1/2}\left(M_s^2 + \frac{2}{\gamma - 1}\right)^{1/2} \tag{4}$$

with the heat capacity ratio $\gamma = 1.4$. θ (see Fig. 1) is the wedge angle at which the invMR → TRR transition occurs. An analysis of Eq. (2) shows that θ increases with the Mach number until $M_s = 2.967$ for which the maximum angle is equal to 68.63 deg. Then θ decreases to an asymptotic value equal to 67.41 degrees. Four different incident shock Mach numbers have been studied: 1.38, 1.8, 2.0 and 3.0. The angles of the invMR → TRR transition are reported in Table 2, showing a good agreement between the theoretical model and computations for $M_s \leq 2$.

IV. Parabolic Reflectors

According to the study of Izumi et al. [2], three types of focalization process may occur when a shock wave impacts a parabolic reflector. The two main parameters are the curvature c of

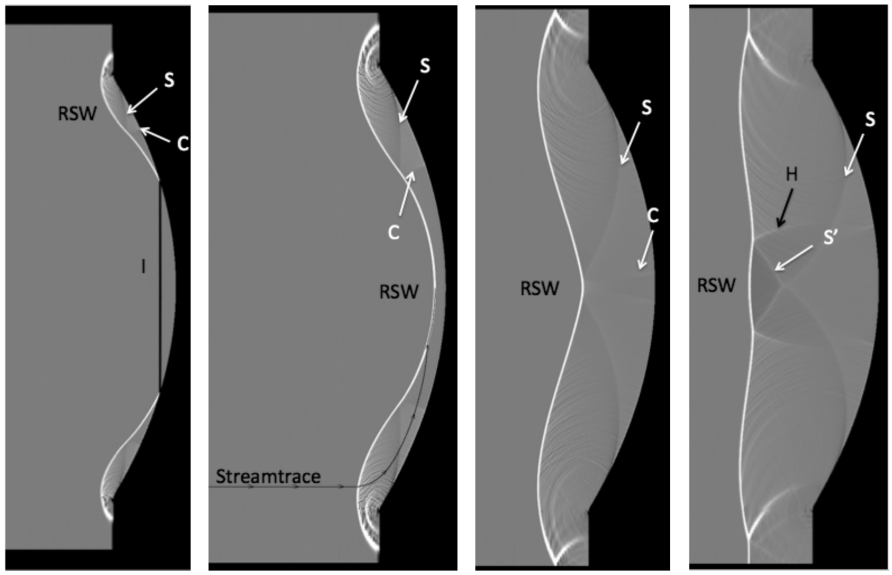

a) BFF b) BFB c) WFP d) AF

Fig. 9 Focusing phenomenon described with a pressure based numerical schlieren contours for a shallow cavity. $M_s = 2$ and $c = 0.75$.

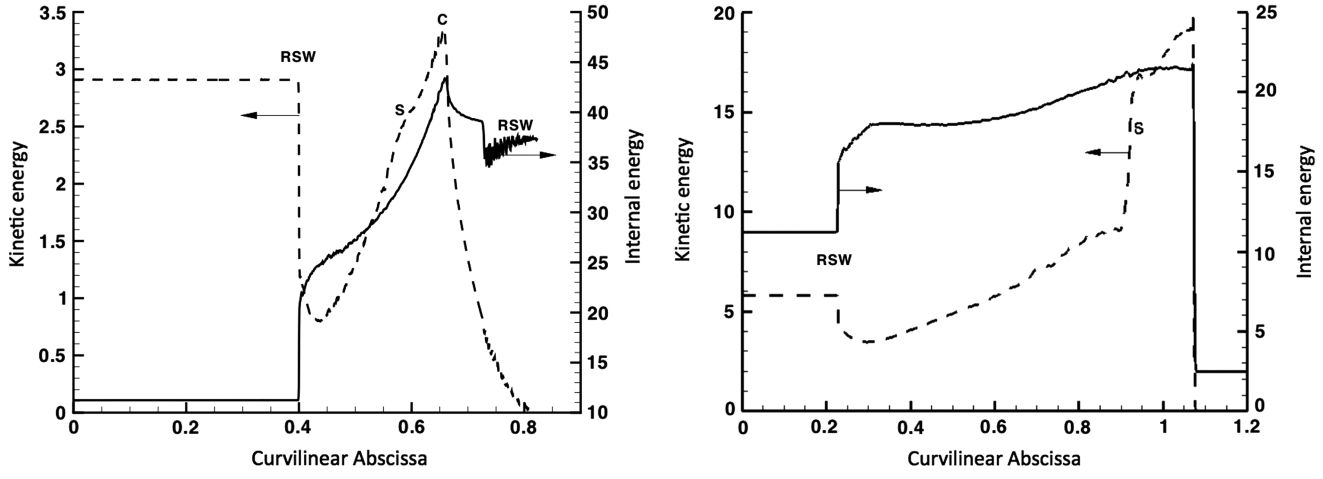

a) Type A b) Type B

Fig. 10 Nondimensional kinetic and internal energies plotted along a given streamline.

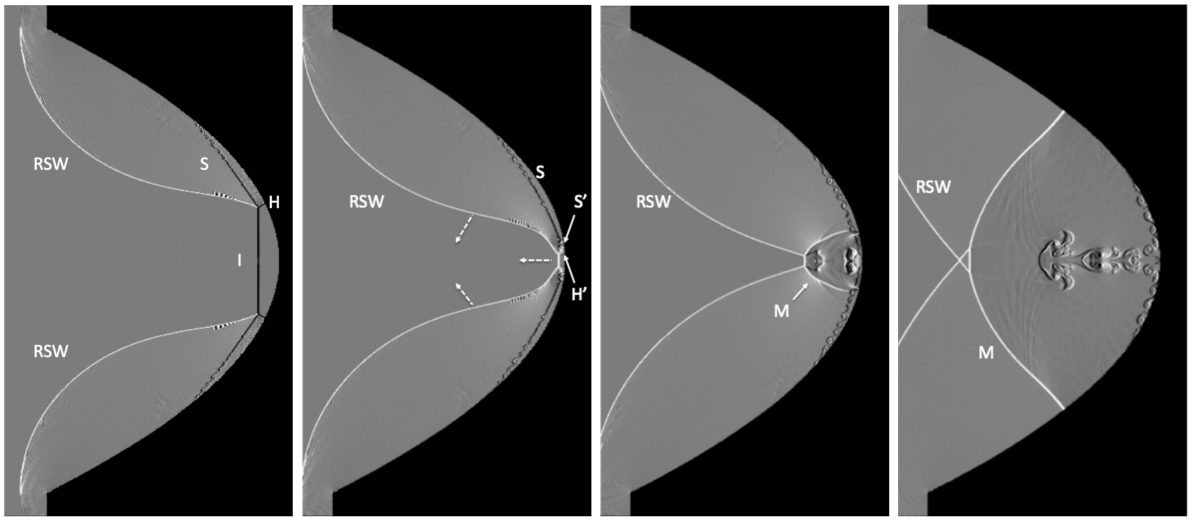

a) b) c) d)

Fig. 11 Focusing phenomenon described with a pressure based numerical schlieren contours at $M_s = 2$ and $c = 1$ for a deep cavity.

reflectors and the incident Mach number M_s. Figure 2b shows the computational domain: parabolic reflectors are defined by their shape, $Y = cX^2$, and depth L. Following Izumi et al. [2], the case $M_s = 2$ and $c = 0.75$ (Euler) is studied hereafter (see Figs. 9a–9d). When the incident shock wave I penetrates inside the cavity, a reflected shock wave (RSW) appears immediately from each side of the cavity and stays connected to the incident shock (Fig. 9a). In the present case, the cavity is shallow and the two RSW intersect each other when the incident wave is reflected (Fig. 9b). This configuration is denoted type A by Izumi et al. [2] and increasing C would lead to the type B configuration, which occurs when the RSW only intersect after the focusing of waves. Type C is defined when the RSW interact before and after the focusing point. The structure of the flow contained between the RSW and the test-piece may be analyzed by plotting E_k and E_i on an instantaneous streamtrace (see Fig. 9b). Results are shown in Fig. 10a and reveal a compression wave (C) and a slipline (S) for any type A configuration. Indeed, C and S are created as soon as I impacts the parabolic reflector but are barely visible in classical numerical schlieren visualizations due to strong numerical or acoustic perturbations (Figs. 9a–9d). They are both

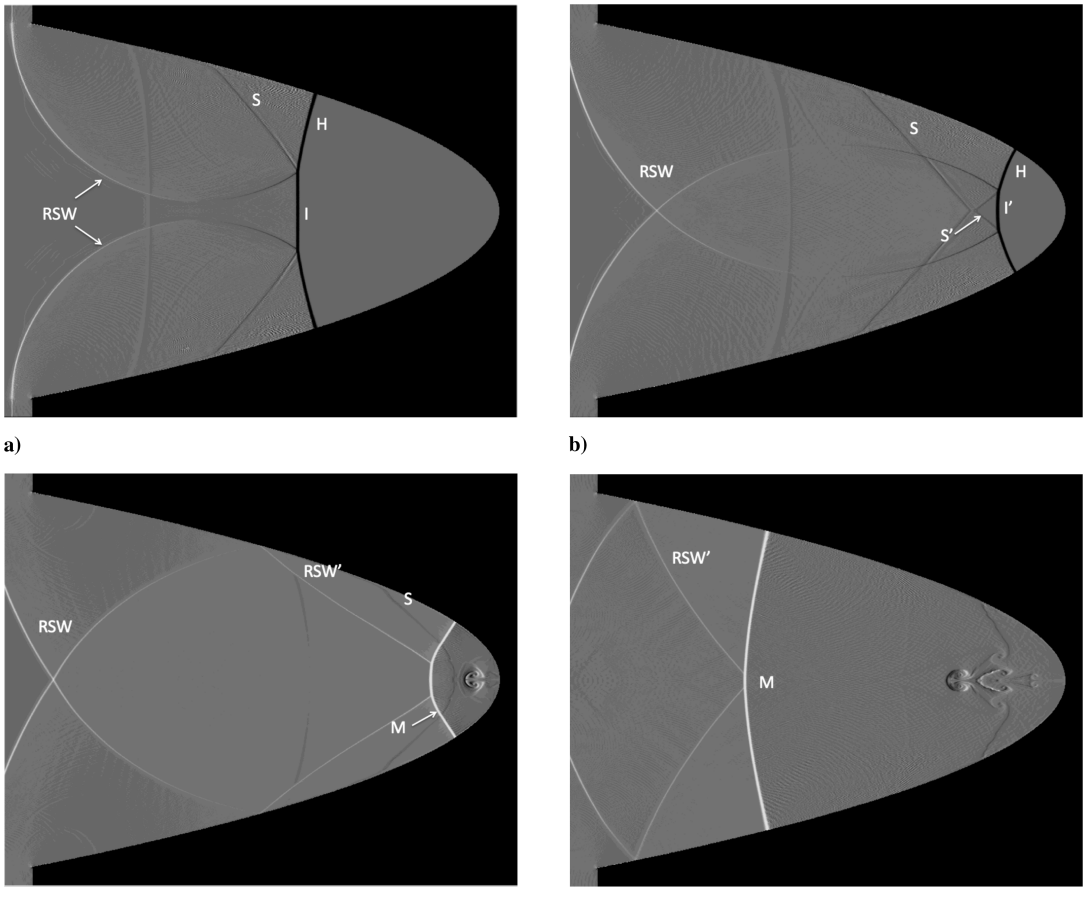

a) b) c) d)

Fig. 12 Focusing phenomenon described with a pressure based numerical schlieren contours at $M_s = 2$ and $c = 1$ for a very deep cavity.

linked to the RSW and move toward the axis of symmetry. Close to the focusing point, the compression waves from each side of the parabola meet (Fig. 9c) and give birth to a small Mach stem (H) (see Fig. 9d). In the meantime, S are detached from RSW and a triple point is created linking H, RSW, RSW′ which is the branch of RSW curved by the Mach stem development and S' which is the new slipline.

According to Izumi et al. [2], increasing the curvature from $c = 0.75$ to $c = 1$ with $M_s = 2$ will change the topology of the flow from a type A to a type B situation. Numerous simulations have been realized and none of them exhibit such a behavior. Nevertheless, type B is recovered when the depth L of the cavity has increased (Figs. 11a–11d) and type C appears when L is much more large (Figs. 12a–12d). For both types, when the incident wave hits the cavity, a single Mach reflection (SMR) appears immediately. Thus, increasing L and keeping constant c and M_s changes the topology of the flow because the angle of attack α (see Fig. 2b) becomes sharper. As a consequence a critical angle α_c depending on c and M_s should exist and separate two distinct phenomena: a compression wave moving lower than the incident shock wave (type A) and a Mach stem attached to the incident shock wave (types B and C).

In the type B configuration (Figs. 11a–11d), the Mach stem H firstly increases as the incident shock progresses into the cavity. E_k and E_i are plotted on a streamtrace again. Figure 10b show the presence of the Mach stem and the slipline. Note that compared with the type A, the jump of E_k is much more high in the case of a SMR. Approaching the bottom of the cavity H decreases and some KH instabilities appears on the slipline S. Near the bottom of the cavity a transition occurs very quickly as the incident shock reflects immediately. The nature of this transition needs a more accurate simulation but these first results tend to show a new SMR structure with a slipline S' attached to S. The incident wave is then reflected but quickly disappears as the two RSW meet each others. At this waves focalization the Mach stems H' of the second SMR structure give birth to a reflected shock and a jet having the shape of a mushroom as in the cylindrical case. Going further into the simulation, the RSW cross once again before being totally separated by the main reflected shock M. In the meantime, the jet evolves facing the entrance of the cavity.

In the type C configuration (Figs. 12a–12d), the length of the cavity is deeper than previously. The curvature and the incident Mach number do not change: $c = 1$ and $M_s = 2$. When I enters into the cavity, the simulations exhibit a SMR structure as in the previous case. However the two RSW have enough time to meet each other before the cavity reflects completely I (Fig. 12a). Before this reflection the 2 M stems H meet and a new triple point is created with a new slipline S' and forwarding shock I' (see Fig. 12b). Approaching the bottom of the cavity, RSW is first reflected by the wall RSW′, immediately followed by I' (Fig. 12c). A main reflected wave M appears and a jet is created in the continuity (Fig. 12d).

V. Conclusions

In this study, Euler and Navier–Stokes computations have been performed to simulate the focusing process of a two dimensional shock wave. High-order low-dissipative shock capturing methods are used to describe accurately both shocks and contact discontinuities and also to assess the performance of different variants of WENO schemes. Overall, accurate results are obtained using the bandwidth-optimized WENO (Martìn et al. [20]) scheme with the limiter proposed by Taylor et al. [21]. The results are qualitatively in good agreement with the experiment of Skews and Kleine [4] in the case of cylindrical reflectors. Furthermore, the computed angles of the invMR → TRR transition compare favorably with the analytical model of Ben-Dor et al. [3] within the limit of weak shock waves ($M_s \leq 2$). In the case of parabolic reflectors, not only the incident Mach number and curvature of the test piece, but also the depth of the cavity, is required to switch from a flow structure to another one. For a shallow cavity, this structure exhibits a compression wave and a slipstream whereas a single Mach reflection appears for a deeper cavity, i.e., with a sharper angle of attack, other things being equal. For the deepest cavities, a KH instability and a jet facing the entrance of the cavity is found similarly to the study of cylindrical cavities. However the nature of these flow structures should be analyzed with more accuracy. Nevertheless, most of the features observed in the experiment are accurately reproduced by the simulations. In general, the results of this study provide a better understanding of the main characteristics of complex shock focusing phenomena that are not easily accessible experimentally, and may be useful for flow controlling and practical shock/obstacle interaction or blast waves design and improvement.

Acknowledgments

This research is supported by the French Aerospace Industry (Snecma-Moteurs/Centre National d'Etudes Spatiales), and the Regional Council of Upper Normandy (Région Haute-Normandie).

References

[1] Grönig, H., "Shock Wave Focusing Phenomena," *Proceedings of the 15th International Symposium on Shock Tubes and Waves*, Stanford Univ. Press, Berkeley, CA, 1986.

[2] Izumi, K., Aso, S., and Nishida, M., "Experimental and Computational Studies Focusing Processes of Shock Waves Reflected from Parabolic Reflectors," *Shock Waves*, Vol. 3, No. 3, 1994, pp. 213–222. doi:10.1007/BF01414715

[3] Ben–Dor, G., *Shock Wave Reflection Phenomena*, Springer–Verlag, New York, 1992.

[4] Skews, B. W., and Kleine, H., "Flow Features Resulting from Shock Wave Impact on a Cylindrical Cavity," *Journal of Fluid Mechanics*, Vol. 580, 2007, pp. 481–493. doi:10.1017/S0022112007005757

[5] Shugaev, F., and Shtemenko, L., *Propagation and Reflection of Shock Waves*, World Scientific, Hackensack, NJ, 1998.

[6] Sturtevant, B., and Kulkarny, V., "The Focusing of Weak Shock Waves," *Journal of Fluid Mechanics*, Vol. 73, No. 4, 1976, pp. 651–671. doi:10.1017/S0022112076001559

[7] Liang, S., Wu, L., and Hsu, R., "Numerical Investigation of Axisymetric Shock Wave Focusing over Paraboloidal Reflectors," *Shock Waves*, Vol. 9, No. 6, 1999, pp. 367–379. doi:10.1007/s001930050167

[8] Gelfand, B., Khomik, S., Bartenev, A., Medvedev, S., Gronig, H., and Olivier, H., "Detonation and Deflagration Initiation at the Focusing of Shock Waves in Combustible Gaseous Mixture," *Shock Waves*, Vol. 10, No. 3, 2000, pp. 197–204. doi:10.1007/s001930050007

[9] Clemens, N., and Mungal, M., "Two- and Three-Dimensional Effects in the Supersonic Mixing Layer," *AIAA Journal*, Vol. 30, No. 4, 1992, pp. 973–981. doi:10.2514/3.11016

[10] Lele, S. K., "Compressibility Effects on Turbulence," *Annual Review of Fluid Mechanics*, Vol. 26, No. 1, 1994, pp. 211–254. doi:10.1146/annurev.fl.26.010194.001235

[11] Ragab, A., and Wu, J., "Linear Instabilities in Two Dimensional Compressible Mixing Layers," *Physics of Fluids*, Vol. A, No. 6, 1989, pp. 957–966.

[12] Zhuang, M., Kubota, T., and Dimotakis, P., "Instability of Inviscid, Compressible Fee Shear Layers," *Physics of Fluids*, Vol. 28, No. 10, 1991, pp. 1728–1733.

[13] Sandham, N. D., and Reynolds, W., "Compressible Mixing Layer: Linear Theory and Direct Simulation," *AIAA Journal*, Vol. 28, 1990, pp. 618–624. doi:10.2514/3.10437

[14] Clemens, N., and Mungal, M., "Large-Scale Structure and Entrainment in the Supersonic Mixing Layer," *Journal of Fluid Mechanics*, Vol. 284, No. -1, 1995, pp. 171–216. doi:10.1017/S0022112095000310

[15] Lesieur, M., Metais, O., and Comte, P., *Large-Eddy Simulations of Turbulence*, Cambridge Univ. Press, Cambridge, England, 2005.

[16] Yee, H., and Harten, A., "Implicit TVD Schemes for Hyperbolic Conservation Laws in Curvilinear Coordinates," *AIAA Journal*, Vol. 25, No. 2, 1987, pp. 266–274. doi:10.2514/3.9617

[17] Skews, B. W., Kleine, H., Barber, T., and Iannuccelli, M., "New Flow Features in a Cavity During Shock Wave Impact," *16th Australian Fluid Mechanics Conference*, Univ. of Queensland, Brisbane, Australia, 2007.

[18] Jiang, G. S., and Shu, C. W., "Efficient Implementation of Weighted Eno Schemes," *Journal of Computational Physics*, Vol. 126, 1996, pp. 202–228.
doi:10.1006/jcph.1996.0130

[19] Shu, C. W., and Osher, S., "Efficient implementation of essentially non-oscillatory shock-capturing schemes ii," *Journal of Computational Physics*, Vol. 83, No. 1, 1989, pp. 32–78.
doi:10.1016/0021-9991(89)90222-2

[20] Martín, M. P., Taylor, E. M., Wu, M., and Weirs, V. G., "A Bandwidth-Hyph-Optimized WENO Scheme for Effective Direct Numerical Simulation of Compressible Turbulence," *Journal of Computational Physics*, Vol. 220, No. 1, 2006, pp. 270–289.
doi:10.1016/j.jcp.2006.05.009

[21] Taylor, E. M., Wu, M., and Martín, M. P., "Optimization of Nonlinear Error for Weighted Essentially Non-Oscillatory Methods in Direct Numerical Simulations of Compressible Turbulence," *Journal of Computational Physics*, Vol. 223, No. 1, 2007, pp. 384–397.
doi:10.1016/j.jcp.2006.09.010

[22] Kudryavtsev, A. N., and Khotyanovsky, D. V., "A Numerical Method for Simulation of Unsteady Phenomena in High Speed Shear Flows," *International Conference on the Methods of Aerophysical Research 98*, International Conference on the Methods of Aerophysical Research, Novosibirsk, Russia, 1998.

[23] Sanders, R., Morano, E., and Druguet, M. C., "Multidimensional Dissipation for Upwind Schemes: Stability and Applications to Gas Dynamics," *Journal of Computational Physics*, Vol. 145, No. 2, 1998, pp. 511–537.
doi:10.1006/jcph.1998.6047

[24] Emanuel, G., *Gasdynamics: Theory and Applications*, AIAA, New York, 1986.

[25] Shi, J., Zhang, Y.-T., and Shu, C.-W., "Resolution of High Order WENO Schemes for Complicated Flow Structures," *Journal of Computational Physics*, Vol. 186, No. 2, 2003, pp. 690–696.
doi:10.1016/S0021-9991(03)00094-9

[26] Samtaney, R., and Pullin, D. I., "On Initial-Value and Self-Similar Solutions of the Compressible Euler Equations," *Physics of Fluids*, Vol. 8, No. 10, 1996, pp. 2650–2655.
doi:10.1063/1.869050

C. Bailly
Associate Editor